ACCEPTED MANUSCRIPT

Impact of fiber distribution and cyclic loading on the bond behavior of steel-reinforced UHPC

YiShao, Katie L.Tich, Sandro B.Boaro, Sarah L.Billington

Cement and Concrete Composites

Received Date: Aug 30, 2020
Accepted Date: Nov 9, 2021
Published Online: Nov 25, 2021

Please cite this article as:

Shao, Y., Tich, K. L., Boaro, S. B., & Billington, S. L. (2021). Impact of fiber distribution and cyclic loading on the bond behavior of steel-reinforced UHPC. *Cement and Concrete Composites*, 104338. DOI: https://doi.org/10.1016/j.cemconcomp.2021.104338

This is a PDF file of a final draft manuscript post-refereeing that has been accepted for publication. The manuscript has completed the peer review process, but this is not the copyedited version of this publication. This publication is provided to promote timely dissemination of scholarly and technical work. Copyright and all rights therein are retained by the authors or copyright holders. Please visit the following website to download the copyedited and published copy of this publication from the publisher:

https://doi.org/10.1016/j.cemconcomp.2021.104338

Impact of Fiber Distribution and Cyclic Loading on the Bond Behavior of Steel-reinforced UHPC

Yi Shao[1], Katie L. Tich[2], Sandro B. Boaro[3], Sarah L. Billington[4]

[1]Ph.D., Dept. of Civil and Environmental Engineering, Stanford University, Stanford, CA 94305. E-mail: yishao@stanford.edu (corresponding author)
[2]Research Assistant, Dept. of Civil and Environmental Engineering, Stanford University, Stanford, CA 94305
[3]Research Assistant, Dept. of Civil and Environmental Engineering, Stanford University, Stanford, CA 94305
[4]Professor, Dept. of Civil and Environmental Engineering, Stanford University, Stanford, CA 94305

Abstract

Ultra-high performance concrete (UHPC) is a class of concrete materials that exhibits high compressive strength (over 150 MPa) and is seeing increasing applications around the world. Current reinforced UHPC (R/UHPC) bond studies mostly adopt non-flexural setups, i.e., pull-out tests and tension-lap-splice tests. The bond behavior of R/UHPC in flexure remains largely unknown, which is a fundamental aspect of designing R/UHPC flexural elements. Additionally, the impact of fiber distribution and cyclic loading on R/UHPC bond is little understood, which is important for guiding the casting and design of R/UHPC structures especially in earthquake zones. This study experimentally investigates the impact of fiber volume, cast flow direction, and cyclic loading on R/UHPC bond behavior under a simulated flexural stress state. Results from twenty-five beam-end tests are discussed. Specimens cast with flow perpendicular to the bar exhibited a 9% to 26% higher bond strength than specimens cast with the flow parallel to the bar due to the resulting higher fiber-bridging capacity across the splitting crack plane. Compared to the monotonically-loaded specimens, cyclic loading minimally impacts R/UHPC bond strength and accelerates bond-degradation after bond softening occurs. Current R/UHPC bond strength prediction methods are evaluated on the test results from this study and the literature. An energy-based R/UHPC bond-slip model is developed. This model captures the cyclic bond degradation of R/UHPC and other types of high-performance fiber-reinforced cementitious composites (HPFRCC) with a mean absolute error under 13%.

Keywords: ultra-high performance concrete; bond behavior; fiber distribution; cyclic loading; fiber volume.

1. Introduction

Ultra-high performance concrete (UHPC), also named ultra-high performance fiber-reinforced concrete (UHPFRC), is an advanced class of concrete that shows high mechanical performance and durability. Mixed with short steel fibers (typically 2% by volume) and designed using packing density theory, UHPC materials generally exhibit tensile and compressive strengths larger than 8 MPa and 150 MPa, respectively, and very low chloride penetration as defined by ASTM C1202 [1]. UHPC materials are often treated as a sub-class of high-performance fiber-reinforced cementitious composite (HPFRCC) because they can sustain increased tensile strength after cracking, i.e., a pseudo-strain hardening phenomenon [2]. UHPC materials are well-suited for applications that need a high strength-to-weight ratio, such as bridges (e.g., [3, 4]), or high corrosion resistance, such as marine structures (e.g., [5, 6]).

The bond behavior of steel reinforced UHPC (R/UHPC) in flexure remains largely unknown (Section 2), which is a fundamental aspect of designing R/UHPC flexural elements. In practice, UHPC materials can flow in different directions around reinforcing bars. Different flow directions can create different fiber orientations around the bars because fiber alignment is predominantly parallel to the flow direction (e.g., [7, 8]) and a fiber-free zone typically exists on the "downstream" side of the bar with perpendicular flow [8]. These different fiber distributions may impact the splitting resistance and therefore R/UHPC bond behavior because the post-cracking behavior of UHPC is contingent on the fiber distribution (e.g., [9, 10]). To the best of the authors' knowledge, the impact of flow-induced fiber distribution on the bond behavior of R/UHPC has not been reported, which is important for guiding the casting and design of R/UHPC structures.

In addition to questions about the impact of fiber distribution on R/UHPC bond behavior, the impact of high-amplitude low-cycle cyclic loading on R/UHPC bond behavior is also not understood. Cyclic loading accelerates the bond deterioration in traditional reinforced concrete (e.g., [11-13]). Since R/UHPC has been proposed for seismic applications (e.g., [14-16]), it is necessary to understand R/UHPC bond behavior under cyclic loading.

In this study, a large-scale experimental program is conducted to investigate the impact of flow direction (i.e., parallel vs. perpendicular to the bar), fiber volume (i.e., 1% vs. 2%), and cyclic loading on the bond-slip behavior of R/UHPC. In total, twenty-five beam-end specimens are tested. In addition to the typical 2% fiber volume, R/UHPC bond behavior with a lower fiber

volume (1%) is explored because recent studies demonstrate that lowering fiber volume improves R/UHPC structural ductility [17]. Finally, current R/UHPC bond strength prediction methods are evaluated on test results from this study and literature. An energy-based R/UHPC bond-slip model is also proposed and validated.

2. Background

In this section, previous studies on bond behavior of R/UHPC are briefly reviewed to support the defined research gaps in Section 1.

The test setups used for determining bond behavior of R/UHPC are categorized into three classes depending on the boundary condition and the stress state of the surrounding material (Fig. 1): pull-out, tension lap-splice, and beam lap-splice. Pull-out tests (Fig. 1a) are widely adopted because of their simplicity but they tend to over-estimate the bond strength. This over-estimation is attributed to the compressive strut that forms between the steel ribs and rigid supports (ACI 408R-03, [18]). Another common setup is the tension lap-splice configuration (Fig. 1b), which replaces the rigid supports by actual reinforcing bars and also represents the reinforcement layout in bridge girder joints. Another way to investigate the bond behavior is by utilizing beam lap-splice configuration (Fig. 1c). In beam lap-splice tests, the rigid supports in traditional pullout tests are avoided, while the surrounding materials are in flexural stress states. Among all three classes of test setup, pull-out tests are considered the least realistic because the compressive stress fields match few cases observed in structural applications [18].

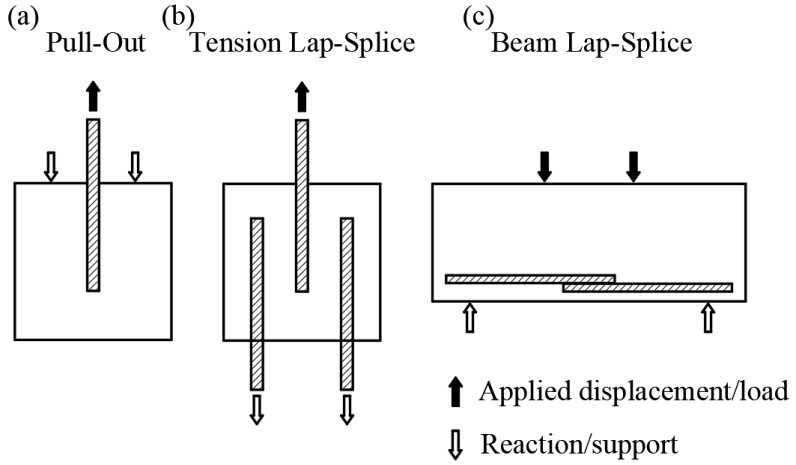

Fig. 1. Current test setups adopted for assessing the bond performance of R/UHPC: (a) pull-out, (b) tension lap-splice, and (c) beam lap-splice.

Fig. 2 presents the results of 117 R/UHPC bond test results reported in the literature in tabulated Appendix A. The test results are classified by the test setup with different bond failure types differentiated i.e., pull-out failures or splitting failures. The reported peak bond strengths range from 6.6 MPa to 76.3 MPa for R/UHPC. Bond strength determined using the pull-out setup is mostly higher than that determined using other types of setup, especially when pull-out type failure is observed. Pull-out type failures are commonly observed from tests with the pull-out setup because of the compressive stress fields [18] and generally large cover thickness (up to 16 d_b in Appendix A, where d_b=bar diameter). A large cover thickness reduces the chance of splitting failures occurring [19, 20] and increases bond strengths [19-23]. After the cover thickness reaches 3-4 d_b, further increase of cover thickness has been found to negligibly impact the bond strength of R/UHPC [21, 24]. There is very little reported data on R/UHPC bond behavior from beam-type tests (Fig. 2), the test setup that provides a more realistic flexural stress state commonly seen in structural members [18].

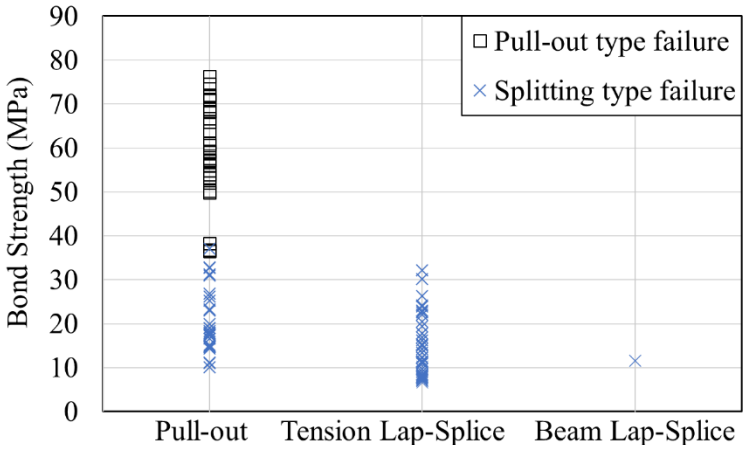

Fig. 2. R/UHPC bond strength test results summary.

The impact of cast-flow-induced fiber distribution on R/UHPC bond strength remains unknown. In previous studies [25, 26], the researchers achieved different fiber orientations by moving casting device over the steel bar(s) following different directions instead of allowing materials flow naturally around the bar. The fiber distribution in their specimens does not replicate natural flow and the resulting fiber distribution including any down-stream side fiber-free zones, which can impact the bond behavior in fiber-reinforced concrete [12].

The embedment length of the test bar in R/UHPC bond tests is often limited to a short length (i.e., 2-5 d_b in Appendix A) for two reasons. First, if the embedment length is too long

(i.e., longer than 6 d_b), the reinforcing bar in the UHPC may fracture before bond failure due to high bond strength [19, 21, 24, 25, 27, 28]. Second, the stress distribution along the embedment length may be non-uniform [20], i.e., most of the bar force is developed within the first $3d_b$ near the loading end [22]. Adopting a short embedment length for these tests avoids underestimating the bond strength. Underestimating R/UHPC bond strength can be unconservative when designing R/UHPC structures because a high bond strength has been found to cause plasticity concentrations and low structural ductility (e.g., [29, 30]).

3. Experimental Program

3.1 UHPC Material

The UHPC studied here is a proprietary material called Ductal and is commercially available from LafargeHolcim (US). The typical composition of Ductal is reported in Ref. [4]. The UHPC material is self-consolidating and densely-packed; the material slump value is around 200 mm, which is measured according to ASTM C1437-15. This UHPC material contains straight steel fibers with a diameter and length of 0.2 mm and 13 mm, respectively. While UHPC materials typically contain a fiber volume of 2%, in our study, we fabricated UHPC with two different fiber volumes: 1% and 2%. The impact of lowering fiber volume on bond behavior is explored because lowering fiber volume from the typical 2% to 1% has been observed to improve structural ductility and also reduces material costs [17, 31, 32]. The materials were mixed based on the material supplier's specified procedure. After casting, the UHPC specimens were moisture cured until 3 days before the test date. If the test age exceeded 56 days, the moisture curing ended at 56 days.

Following ASTM C1856-17 [33], the compressive and flexural behavior of the materials were assessed using cylinder and unreinforced beam tests. The cylinders were 76 mm in diameter and after end-grinding, on average 141 mm high, and were subject to uniaxial compression. The unreinforced beams had a cross-section of 76 mm by 76 mm and were 280 mm long. They were subjected to third-point bending across a span of 228 mm. Fig. 3 presents a representative result of the four specimens tested for each material characterization test. Fig. 4 illustrates the development of material strength with test ages of 28 days, 56 days, and 168 days. Table 1 gives the measured material properties at 28-days. Detailed descriptions of the material characterization test setup and results are available in [17].

Table 1 UHPC Properties at 28 days

	f'_c (MPa) Mean (std) [#]	$\sigma_{flexure}$ (MPa) Mean (std) [#]	f_t (MPa)
UHPC-Vf2%	174.0 (6.1) [*4*]	24.3 (1.2) [*4*]	9.9
UHPC-Vf1%	172.7 (5.3) [*4*]	17.1 (2.3) [*4*]	6.7

Note: f'_c=compressive strength; $\sigma_{flexure}$=equivalent bending strength from unreinforced beam tests; f_t=tensile strength estimated form unreinforced beam tests using an inverse analysis [17]; std=standard deviation, #=number of tests conducted.

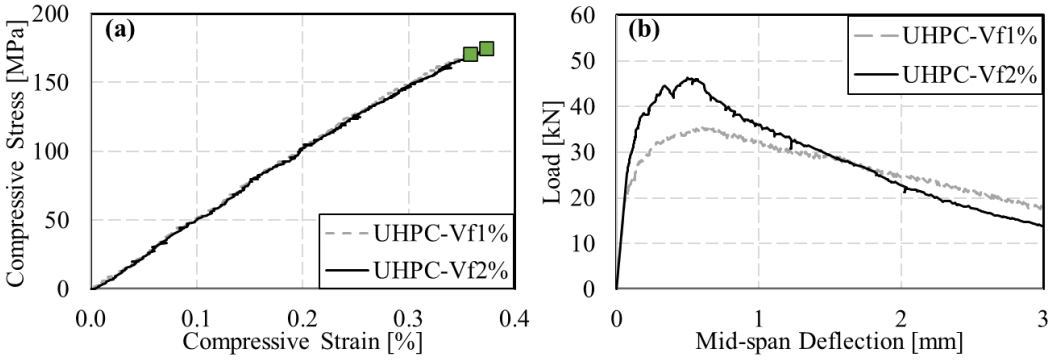

Fig. 3. Representative results from material characterization tests: (a) cylinder compression tests, and (b) unreinforced beam tests. '□' explosive failure.

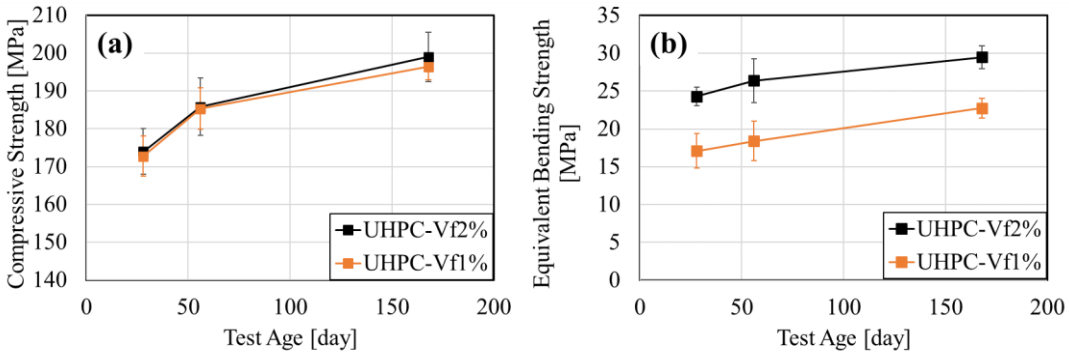

Fig. 4. Development of UHPC (a) compressive strength and (b) equivalent bending strength. Note: vertical error bars represent standard deviation.

3.2 Beam-end Specimen Design

Based on recommendations from ACI committee 408, bond-slip is studied here using beam-end tests, which provide realistic flexural stress states commonly seen in structural members [18]. For both conventional concrete and fiber-reinforced concrete, the bond strength determined from

beam-end tests has been found to represent well the response seen in beam lap-splice experiments (e.g., [12, 18]). Fig. 5 presents the specimen design. This specimen design follows ASTM A944-10 [34] and is similar to Bandelt et al. [12].

The specimens were 380 mm high, 130 mm wide, and 230 mm long. The test bar was a 16-mm-diameter steel bar with a bonded length of $3d_b$ (d_b=bar nominal diameter). This bonded length was chosen because a longer bonded length is expected to cause steel failure before bond failure (reviewed in section 2), and a shorter bonded length could lead to large uncertainties by including too few ribs ([25, 35]). Table 2 lists the properties of the test bar, and Fig. 6 provides the steel stress-strain relationship measured from uniaxial tension tests.

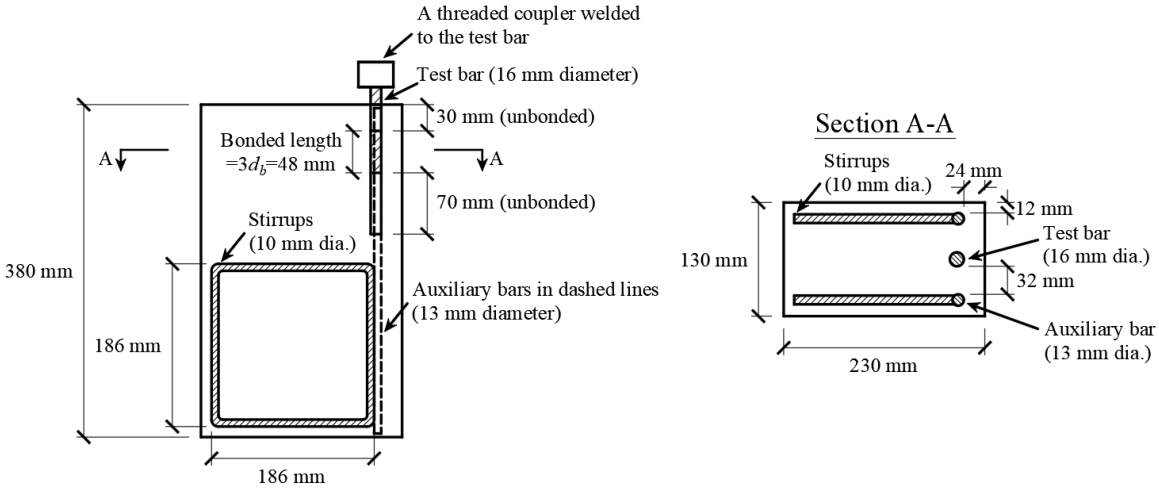

Fig. 5. Beam-end specimen design.

Table 2 Test bar properties

Property	Unit	Value
Elastic Modulus	GPa	202
Yield strength	MPa	470
Ultimate strength	MPa	674
Nominal diameter	mm	16
Rib height*	mm	1.2
Rib spacing*	mm	10.6
Relative rib area*	-	0.096

Note: *Surface deformation is measured according to ACI 408R-03

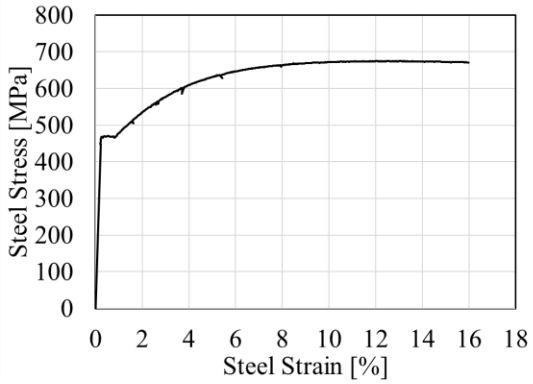

Fig. 6. Steel stress-strain relationship. Note: the steel strain was measured using an extensometer with a 50-mm gage length.

Outside the bonded region, the test bar was wrapped with duct tape and sealed in a PVC tube to create unbonded regions above and below. As suggested by ASTM A944-10 [34] and ACI 408R-03 [18], the loaded end of the test bar had an 30-mm-long unbonded region to avoid a localized cone-type failure. The unloaded end of the test bar extended 40 mm into the 70-mm-long PVC tube (Fig. 5) to allow cyclic slip.

Two auxiliary steel bars with a diameter of 13 mm were provided to control flexural cracks that could develop outside the bonded region (Fig. 5). Two 10-mm-diameter stirrups parallel to the side faces were provided as shear reinforcement. The cover thickness in current UHPC applications ranges from 20 mm to 30 mm. Therefore, a bottom cover thickness of 24 mm was chosen, resulting in a bottom cover-to-bar-diameter ratio of 1.5.

3.3 Casting Method

The flow direction of the fresh UHPC paste was either parallel or perpendicular to the test bar (Fig. 7). The parallel flow was achieved by allowing the material to flow from the back of the form to the other end until the entire form is filled (Fig. 7a). The perpendicular flow was achieved in two steps. In the first step, the material was placed to flow from one side of the form to the other with three specimen reinforcing cages side by side (Fig. 7b). After the form was filled by the natural flow of the material placement until over half of its height, vertical separators were inserted, and the first step was completed. In the second step, the rest of the specimen was filled by moving the casting device back and forth over the form while slowly

placing the additional material without introducing material flow. Extreme caution was paid to avoid disturbing the fiber distributions generated by the perpendicular flow in the first step.

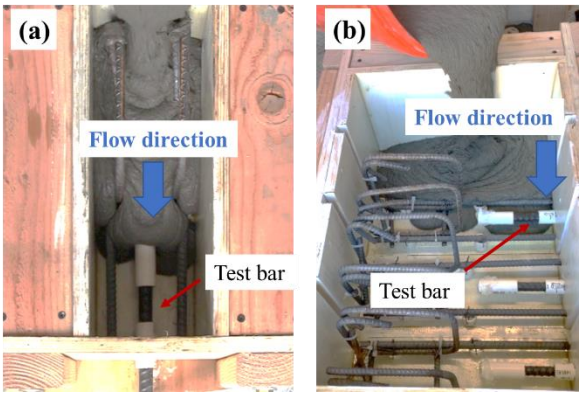

Fig. 7. Photos of the casting methods: (a) materials flow parallel to the bar, and (b) materials flow perpendicular to the bar.

3.4 Beam-End Test Setup and Loading Protocol

Fig. 8 presents a schematic of the test setup. The test bar was loaded by the actuator of a 245 kN MTS machine at a displacement-controlled rate of 0.008 mm/s. Two linear variable differential transformers (LVDTs) were clamped to a coupler that was welded to the test bar, measuring the displacement of the clamping point against the top surface of the specimen (Fig. 8). Readings from these two LVDTs were averaged to obtain the clamping-point displacement, which consisted of bond slip and the steel deformation between the clamping point and loaded end of the test bar. The beam-end specimen movement was restrained by six steel rods and the

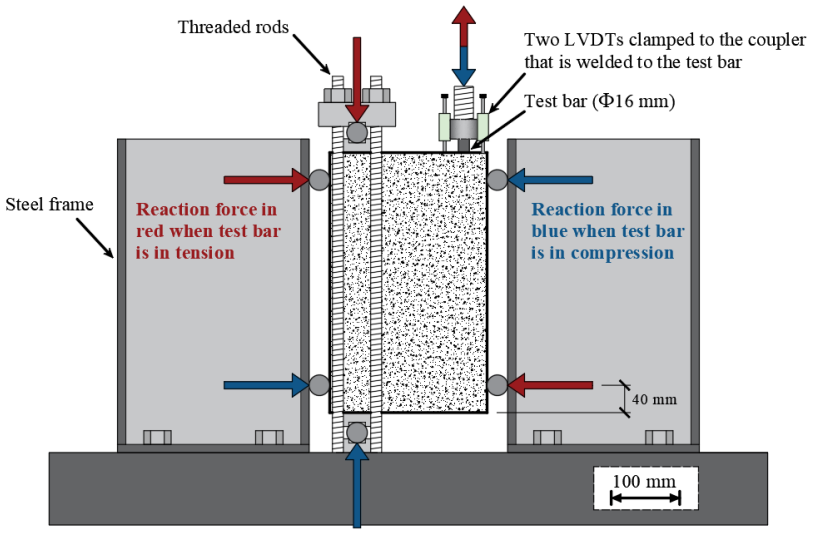

Fig. 8. Overview of the beam-end test setup.

surrounding rigid steel frames. No support preload is applied, while the expected reaction force is shown in Fig. 8.

For the monotonic tests, the test bar was pulled in tension. For the cyclic tests, the specimen was first subjected to load-controlled cycles in tension and compression and then displacement-controlled cycles (Fig. 9). Note that, in this study, positive load and slip values represent when the test bar was in tension. In the load-controlled protocol, two cycles were exerted at 50%, 65%, 80%, and 90% of the average peak bond strength, u_{max}, from monotonic tests (Fig. 9a). The displacement-controlled protocol started when the load-controlled protocol was complete or when the reinforcement slip exceeded 1 mm, whichever occurred first. The displacement-controlled protocol consisted of two cycles at 1, 2, 3, and 4 mm displacement (Fig. 9b). After the displacement-controlled protocol was complete, the test bar was monotonically pulled in tension until 10 mm slip.

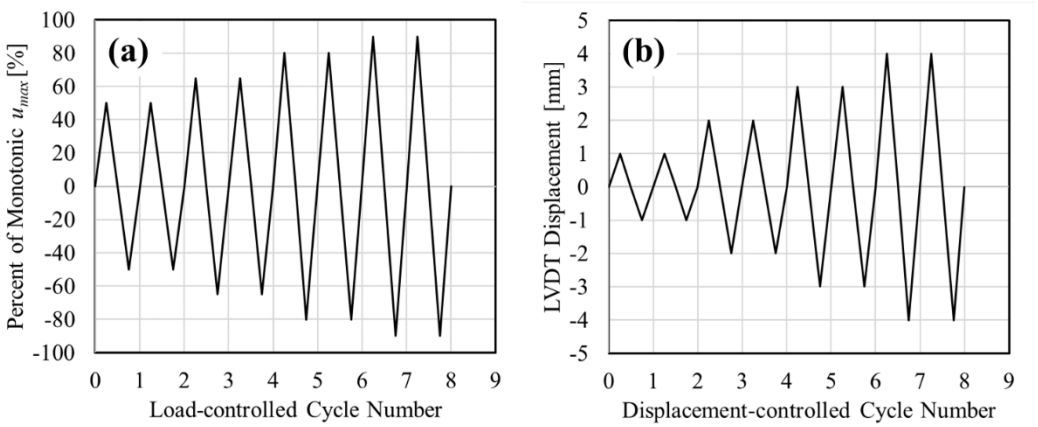

Fig. 9. Cyclic loading protocol of (a) load-controlled cycles, and (b) displacement-controlled cycles.

3.5 Test Matrix

Table 3 presents the test matrix. Most of the monotonic specimens were tested at 28±2 days, while the remainder of the specimens were tested at 100±2 days due to an unexpected lab shutdown. The naming convention includes fiber volume, flow direction, loading type, and test age.

Table 3 Test matrix

Combination	V_f [%]	Flow direction	Loading	Test age (day)	N_{test}
UHPC-Vf2-PL-M-28D	2	Parallel	Monotonic	28	4
UHPC-Vf2-PD-M-28D	2	Perpendicular	Monotonic	28	5
UHPC-Vf1-PL-M-28D	1	Parallel	Monotonic	28	4[a]
UHPC-Vf1-PD-M-28D	1	Perpendicular	Monotonic	28	3
UHPC-Vf2-PL-M-100D	2	Parallel	Monotonic	100	1
UHPC-Vf2-PL-C-100D	2	Parallel	Cyclic	100	2
UHPC-Vf2-PD-M-100D	2	Perpendicular	Monotonic	100	1
UHPC-Vf2-PD-C-100D	2	Perpendicular	Cyclic	100	2
UHPC-Vf1-PL-C-100D	1	Parallel	Cyclic	100	3

Note: V_f=fiber volume, [a]=LVDTs were malfunctioning for one of the four tests, therefore the bond-slip curve for just three tests are reported. N_{test}=number of tests conducted for this combination.

4. Bond Experimental Results and Discussion

Table 4 summarizes the test results. The bond stress, u, is calculated assuming a uniform stress distribution:

$$u = \frac{P}{\pi \cdot d_b \cdot l_{bond}} \quad (1)$$

,where P=external load on the test bar (positive when the test bar is in tension), l_{bond}=bonded length (48mm), d_b=bar diameter (16 mm).

Table 4 Summary of test results

Combination	u_{max} [MPa] Mean (Std.)	$\omega_{s,max}$ [mm] Mean (Std.)	N_{test}
UHPC-Vf2-PL-M-28D	32.6 (3.8)	1.1 (0.3)	4
UHPC-Vf2-PD-M-28D	41.0 (1.2)	0.5 (0.3)	5
UHPC-Vf1-PL-M-28D	29.9 (3.0)	1.4 (0.3)	4
UHPC-Vf1-PD-M-28D	32.6 (2.8)	1.3 (0.1)	3
UHPC-Vf2-PL-M-100D	38.6 (N/A)	1.0 (N/A)	1
UHPC-Vf2-PL-C-100D	39.8 (0.8)	0.8 (0.4)	2
UHPC-Vf2-PD-M-100D	45.2 (N/A)	0.5 (N/A)	1
UHPC-Vf2-PD-C-100D	43.3 (0.7)	0.6 (0.2)	2
UHPC-Vf1-PL-C-100D	32.0 (2.1)	0.8 (0.1)	3

Note: u_{max}=bond strength, $\omega_{s,max}$=maximum residual splitting crack width that is manually measured by a caliper after the tests. Std.=standard deviation. N_{test}=number of tests conducted for this combination. N/A=not applicable.

4.1 Crack Pattern and Failure Mode

Fig. 10a shows the representative crack pattern of a beam-end specimen after the test bar was completely pulled out. The crack pattern consisted of splitting cracks that were parallel to the test bar axis and flexural cracks that were perpendicular to the test bar axis. Despite the lack of stirrup confinement, R/UHPC bond failure was gradual and considered as confined splitting failure. The fiber-bridging of the UHPC material restrained the splitting cracks, causing the UHPC keys between the steel ribs to shear off and be pulverized for all specimens (see representative test bar after failure in Fig. 10b). No steel fiber was found in the sheared-off keys. Ongoing studies reveal that although UHPC matrix is compact around the reinforcing bar regardless of the flow directions [36], a fiber-free zone exists between the steel ribs. In contrast, for traditional concrete without stirrup confinement, splitting bond failures feature a sudden load drop when the concrete separates from the bar. Concrete keys between steel ribs typically do not shear off (e.g., [13, 37]).

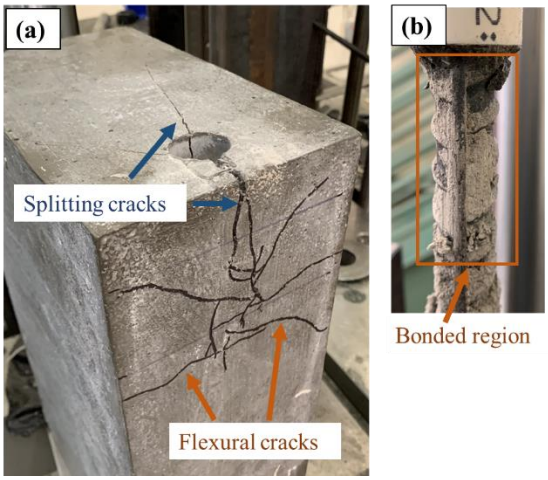

Fig. 10. Photos of (a) a representative crack pattern, and (b) a completely-pulled-out test bar.

4.2 Monotonic Bond Behavior

Fig. 11 presents the bond-displacement responses of the monotonically-loaded specimens, while the determined bond strength and maximum residual splitting crack width are given in Table 4. The displacements in Fig. 11 are the averaged readings from the two LVDTs. The bond-displacement relationship is shown here because the test bar yielded in some specimens; the bond-slip relationship is provided in section 5 when discussing the bond-slip model.

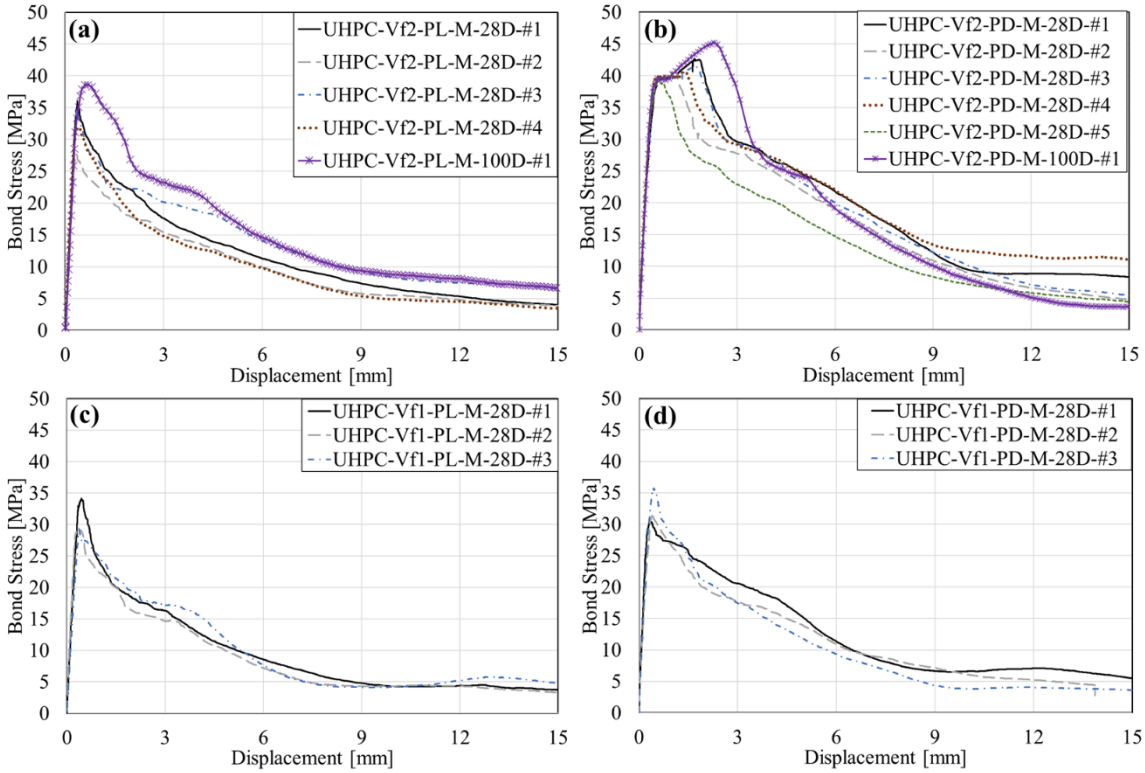

Fig. 11. Bond-displacement responses for specimens with (a) 2% fiber volume and parallel flow, (b) 2% fiber volume and perpendicular flow, (c) 1% fiber volume and parallel flow, and (d) 1% fiber volume and perpendicular flow.

Specimens from all four combinations showed a mixed splitting and pull-out failure, as discussed in section 4.1. For specimens in Figs. 11a&c&d, their bond stress kept increasing until visible splitting cracks formed. Bond failure occurred quickly after the formation of the splitting cracks. The bond failure was gradual since fiber-bridging in the UHPC restrained the splitting cracks. Further slip was accompanied by shearing off the UHPC keys between steel ribs, as discussed previously (Fig. 10b). For specimens in Fig. 11b, bond stress kept increasing after the splitting crack formed. The test bar yielded when the bond stress reached 39 MPa, resulting in a strength plateau. Test bar yielding is common in R/UHPC bond tests due to their high bond strength (e.g., [21, 23, 25, 27, 38]). After the yielding plateau, the bond stress continued to increase until a gradual pull-out failure occurred.

Similar to the bond strength in reinforced concrete [39], the bond strength of R/UHPC also depends on the confinement provided, which is affected by the fiber volume and flow direction. In UHPC, the fiber alignment is mostly parallel to the flow direction (e.g., [7, 10, 40]). Therefore, the combination of 2% fiber volume and perpendicular flow was expected to generate

the highest fiber-bridging capacity across the splitting crack planes, which are parallel to the bar axis (Fig. 10a). The higher splitting resistance was observed in the average residual splitting crack widths measured ($\omega_{s,max}$ in Table 4). For the specimens tested at 28 days, the crack width for combination UHPC-Vf2-PD is 55%-65% smaller than that observed in the other three combinations. As a result, the combination of 2% fiber volume and perpendicular flow generated the highest bond strength among the four combinations (Table 4). Meanwhile, the combination of 1% fiber volume and parallel flow showed the lowest bond strength as expected, since this combination brought the lowest fiber-bridging capacity across the splitting crack plane among the four combinations.

These results demonstrate that flow direction and fiber volume affect R/UHPC bond strength under flexural states due to the change in splitting resistance. For the specimens tested at 28 days, when the fiber volume was the same, changing the flow direction from parallel to perpendicular increased the average bond strength by 9% and 26% for 1% fiber volume and 2% fiber volume, respectively. For the same flow direction, increasing the fiber volume from 1% to 2% increased the average bond strength by 9% and 26% for parallel flow and perpendicular flow, respectively (Table 4).

Note that, the average bond strength is almost same for UHPC-Vf2-PL-28D and UHPC-Vf1-PD-28D, which is attributed to their having a similar splitting resistance (i.e., similar tensile strength across the splitting plane). Compared to UHPC-Vf2-PL-28D, which has a high fiber volume (2%) and flow direction parallel to the splitting crack plane, UHPC-Vf1-PD-28D has a lower fiber volume (1%) and flow direction perpendicular to the splitting crack plane. Similar splitting resistance in specimens UHPC-Vf2-PL-28D and UHPC-Vf1-PD-28D is assumed based on: (1) uniaxial tension tests demonstrate that the fiber-bridging capacity across a plane that is perpendicular to the flow direction is 68%-127% higher than that across a plane parallel to the flow direction [10], and (2) uniaxial tensile strength of UHPC with 2% fiber volume has been found to be 46%-131% higher than that with 1% fiber volume [1, 26]. Based on these results, it is reasonable to consider that UHPC-Vf2-PL-28D may have lower splitting resistance based on flow direction but higher splitting resistance based on fiber volume fraction, leading to the assumption that it's splitting resistance would be roughly the same as that of UHPC-Vf1-PD-28D.

When compared to specimens tested at 28 days, specimens with the 100-day age show a bond strength increase of roughly 6-7%. This bond strength increase is attributed to the coupled effects of increased compressive strength (i.e., stronger UHPC keys, Fig. 4a) and increased fiber bridging capacity (i.e., higher splitting resistance, Fig. 4b). A larger-scale program is underway to further investigate the impact of material properties on UHPC bond behavior.

4.3 Cyclic Bond Behavior

Fig. 12 compares the cyclic bond-displacement responses to the monotonic responses. In Figs. 12a-d, the pre-softening cyclic responses are denoted using red-dotted lines indicating steel hysteresis, while the post-softening cyclic responses are shown with black solid lines representing cyclic bond-slip behavior, as discussed further below. For Figs. 12e-g, monotonic tests were not performed at the same age, so the averaged responses from 28-day specimens are provided in Figs. 12e-g. Note that, the 100-day bond strength is expected to increase from 28-day strength as discussed in section 4.2.

For all cyclic specimens, the responses during load-controlled cycles followed linear unloading-reloading branches through the origin. No noticeable stiffness degradation was observed at this stage. The pre-peak load cycles were not found to impact the maximum bond strength. The mean absolute difference between the maximum bond strength of cyclic specimens and monotonic specimens is 0.8 MPa, which is within the variance between specimens (Fig. 11 and Table 4).

Similar to the trends with monotonic bond-slip behavior, increasing the fiber volume from 1% to 2% or changing the flow direction from parallel to perpendicular increased the average bond strength by 9% to 35%. For specimens with UHPC having 2% fibers by volume (Fig. 12a-d), their bond-displacement hysteresis between the yielding point of the test bar and the point at which bond softening began (i.e., these red dotted lines) was dominated by steel cyclic hysteresis. When softening began, the bond-displacement hysteresis (i.e., these black solid lines in Fig. 12) is attributed to bond-slip behavior because the steel stress is kept below the yielding stress.

Fig. 13 presents a schematic of a typical bond-slip cycle after bond softening has initiated in reinforced UHPC in 5 steps:

322

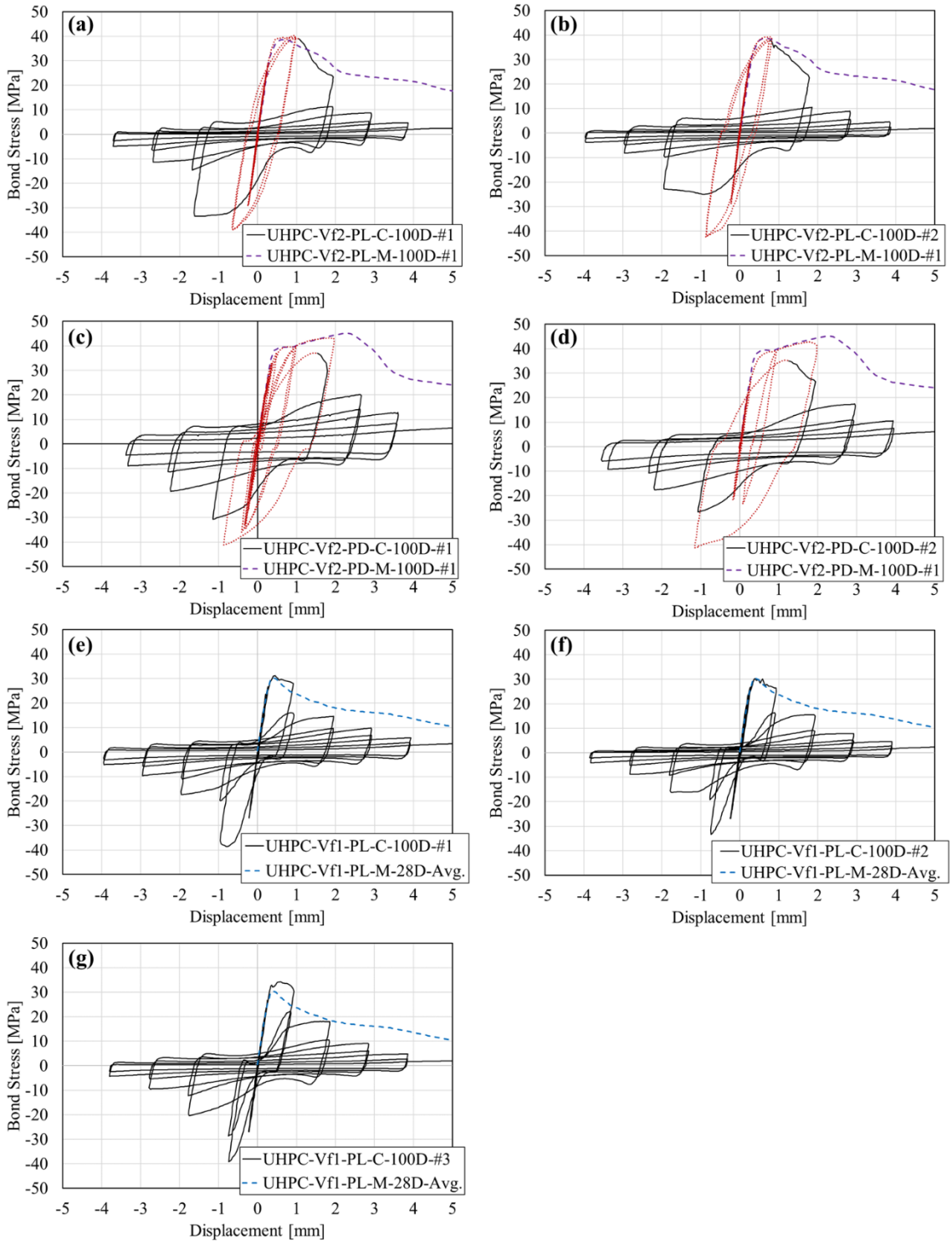

Fig. 12. Bond-displacement responses of specimens with 2% fiber volume cast parallel (a-b), specimens with 2% fiber volume cast perpendicular (c-d), and specimens with 1% fiber volume cast parallel (e-f). Note: for a-d, pre-softening cyclic behavior is represented using red dotted lines.

1. When the first slip reversal starts at point C, the steel rib is pushed against the right bearing surface with inclined shear cracks that are hypothesized to have already formed [13]. When the slip is reversed from point C, a stiff unloading branch first occurs (point C to D). At this stage, the steel rib is still in contact with the UHPC key, while the UHPC elastic deformation is recovered and some frictional resistance is built.
2. From point D to E, the steel rib slides through the left gap. The bond stress gradually increases as some broken UHPC pieces start transferring load between the steel rib and UHPC key.
3. When the slip reaches point H, new damage is introduced to the left bearing surface in the form of new bond cracks and crushed UHPC. Again, a slip reversal first introduced a stiff unloading branch from H to I.
4. Similar to the path D-E, the steel rib slides from point I to J with increasing bond stress.
5. When the slip reaches the same slip as point C (i.e., reaches point J in Fig. 13), the bond stress is lower than that of point C because the UHPC keys gain additional damage from the previous cycle.

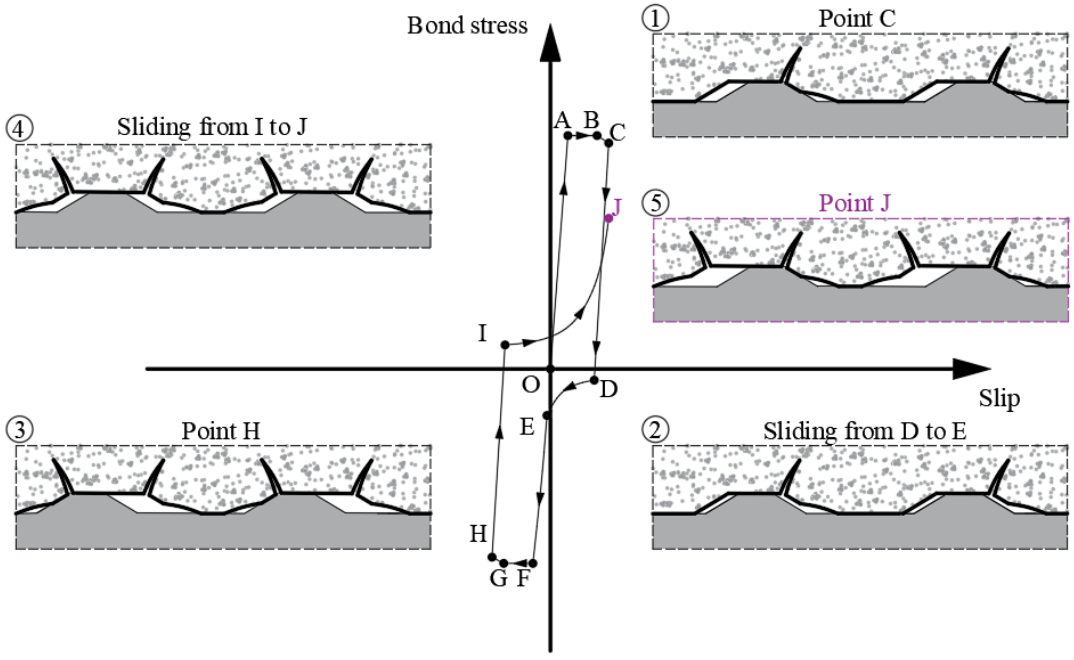

Fig. 13. Schematic of a typical bond-slip cycle.

Therefore, repeated slip reversal accelerates bond degradation, as observed in Fig. 14. This accelerated bond degradation has also been observed in previous cyclic bond tests of concrete (e.g., [13]), fiber-reinforced concrete (e.g., [11]), and other types of HPFRCC [12].

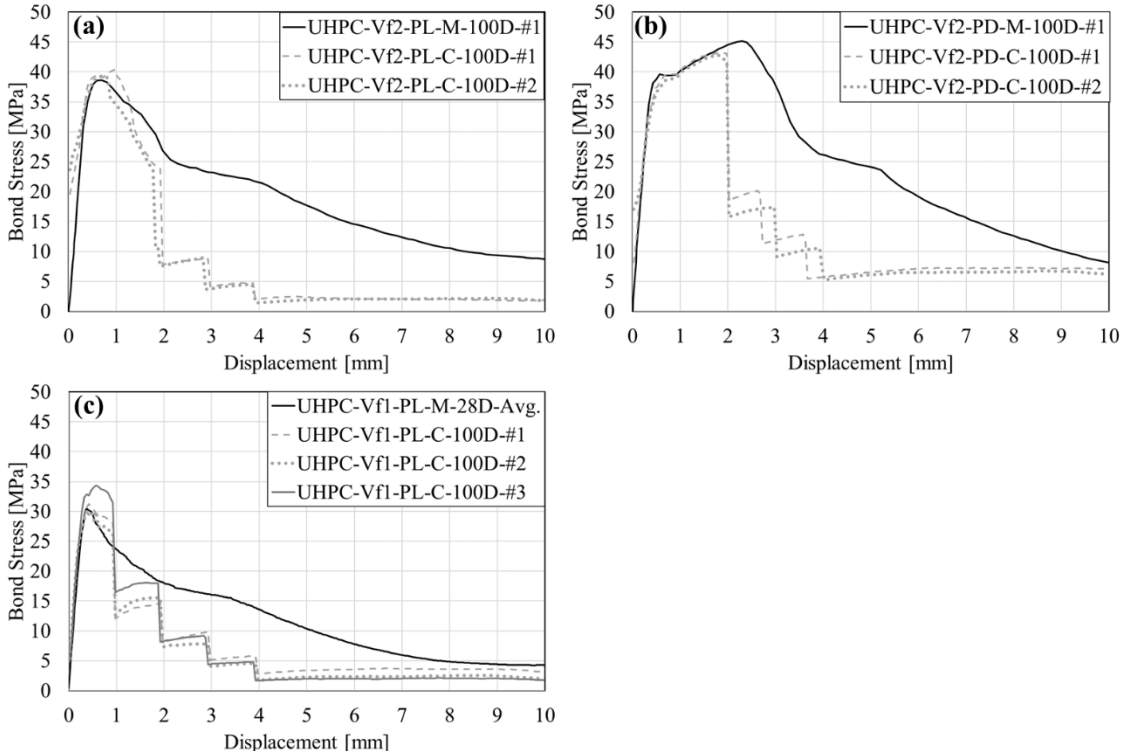

Fig. 14. Load-displacement envelope of specimens with (a) UHPC-Vf2-PL, (b) UHPC-Vf2-PD, and (c) UHPC-Vf1-PL.

5 Predicting R/UHPC Bond-slip Behavior

In this section, current methods for predicting R/UHPC bond strength are first evaluated. Then, an R/UHPC bond-slip model is proposed and validated to capture the general envelope of monotonic bond behavior as well as cyclic bond degradation.

5.1 Predicting R/UHPC Bond Strength

This section evaluates current R/UHPC bond strength prediction methods by comparing the predicted results to experimental results from this study as well as the collected dataset (Appendix A).

As reviewed in section 2, a large range of R/UHPC bond strength (from 6.6 MPa to 76.3 MPa) has been reported in the literature. In addition to the already-identified factors (e.g., embedment length and cover thickness as reviewed in section 2), Fig. 2 indicates that the test

setup (i.e., stress states) impacts R/UHPC bond strength. Additionally, the experimental results in section 4 demonstrate that material flow direction and fiber volume also noticeably affects the bond strength. While no existing bond strength method considers all the aforementioned factors, Fig. 15 presents the prediction performance of current R/UHPC bond models [20, 26, 35] applied to the database of experiments presented in this study and Appendix A. Table 5 provides details of the existing models as well as summarizes the mean absolute prediction error of the test results from each type of test setup. Note that in Fig. 15 and Table 5, the beam-type test results are primarily from this study with one additional datapoint from [41].

Table 5 R/UHPC Bond Strength Prediction Models and Prediction Errors

Model Name	Source Tests for the Model	Model	Mean Absolute Prediction Error		
			Pull out	TLS	Beam
Yoo model [35]	Pull out tests	$u_{max} = 5\sqrt{f_c'}$	37.7%	440.0%	151.6%
Sturm model [20]	Pull out tests	$u_{max} = (0.0018 \cdot \mathrm{c}{+}0.186) \cdot f_c$	40.0%	184.4%	45.7%
Roy model [26]	TLS tests	$u_{max} = (0.45 \cdot \frac{c}{d_b} + \frac{38.5}{l_b} + 0.23 \cdot V_f) \cdot f_t$	53.5%	24.0%	56.4%

Note: TLS=Tension lap splice. Other notations in the bond strength prediction equations are explained in Appendix A.

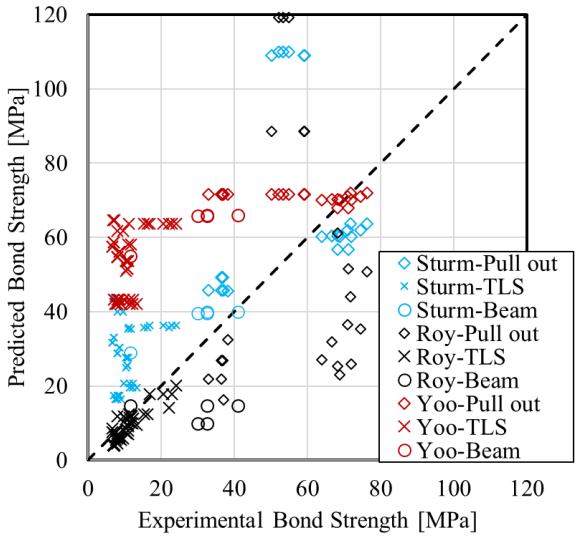

Fig. 15. Comparison between experimental and predicted R/UHPC bond strength through application of the models described in Table 4 to the experiments presented in this study and Appendix A. Note: TLS=Tension lap-splice.

Overall, these three R/UHPC bond strength models show the smallest prediction error on tests that share a similar test setup as their source tests, as expected. Since the Yoo model is a function of compressive strength, which does not vary significantly across tests, it captures the least bond strength variation among the three models (Fig. 15). The Yoo model also tends to

368 overpredict R/UHPC bond strength, especially for test results from tension-lap-splice type tests.
369 The Sturm model and the Roy model better capture the bond strength variation (Fig. 15). Note
370 that, when the cover thickness is high (e.g., c/d_b=16.2 in [21]), both the Sturm model and the Roy
371 model predict a very high bond strength from 88 MPa to 119 MPa, which is over 100% higher
372 than the test results.
373 For the beam-type test results, all three models exhibit a mean absolute error higher than
374 45%. Further studies are needed to develop a more comprehensive bond-strength prediction
375 model that better captures the effects of material properties and stress states, especially the
376 flexural stress states in beam-type tests.
377
378 ***5.2 Proposed R/UHPC Bond-slip Model***
379 Fig. 16 presents a proposed R/UHPC bond-slip model. The monotonic envelope generally
380 follows the suggestions from the *fib* Model Code [39]. The monotonic envelope consists of (1) a
381 linear ascending branch up to point A, (2) a strength plateau from point A to B, (3) a linear
382 descending branch to point M, and (4) a plateau representing a residual strength after point M.
383 The monotonic envelope is defined by the following equations:

384 $$u(s)=\begin{cases}\frac{s}{s_1}u_{max} & ,0\le s\le s_1\\ u_{max} & ,s_1\le s\le s_2\\ u_{max}-\frac{u_{max}-u_{bf}}{s_3-s_2}(s-s_2) & ,s_2\le s\le s_3\\ u_{bf} & ,s_3\le s\end{cases} \quad (2)$$

385 ,where $u(s)$=bond stress at the slip value of s, s_1=0.2 mm; s_2=0.5 mm; s_3=clear distance between
386 ribs (i.e., 8mm in this study, [39]); u_{max}=maximum bond stress, MPa; u_{bf}=residual bond
387 frictional resistance, MPa. Based on the monotonic tests reported herein, u_{bf} is estimated as 20%
388 of the u_{max}.

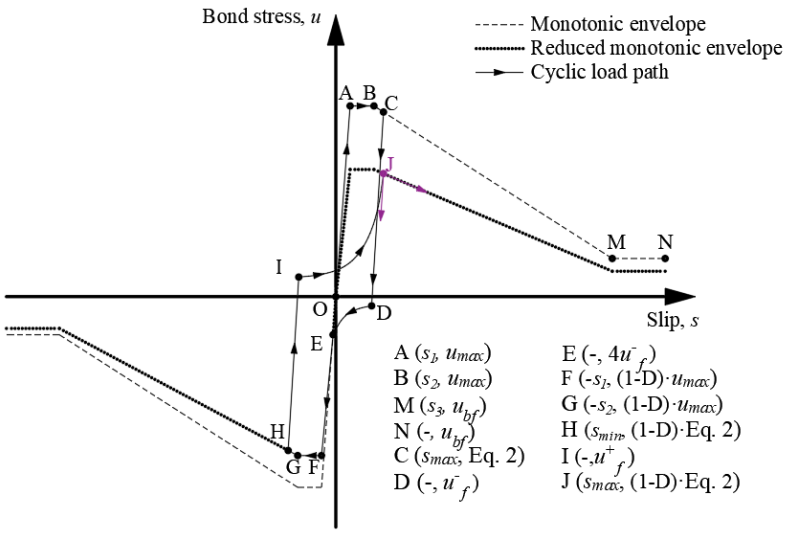

Fig. 16. Schematic of the proposed R/UHPC bond-slip model.

The proposed model considers the cyclic effects based on the test results in this study and a widely-adopted framework first proposed by Eligehausen et al. [13], which successfully predicts the concrete cyclic bond-slip behavior. Before reaching point A, the cyclic bond-slip behavior follows linear unloading-reloading paths through the origin with the same stiffness as the original ascending branch. After reach point A, this model considers the cyclic bond degradation using an energy-based damage index, D. This damage index, D, is calculated as:

$$D = 1 - e^{-1.8\cdot(E/2\cdot E_0)^{0.8}} \quad (3)$$

, where E is the accumulated dissipated energy before the slip reversal begins, and E_0 is the dissipated energy during monotonic loading (Fig. 17). The damage index (Equation 3) was obtained based on a regression analysis of the test results of the specimens in combination

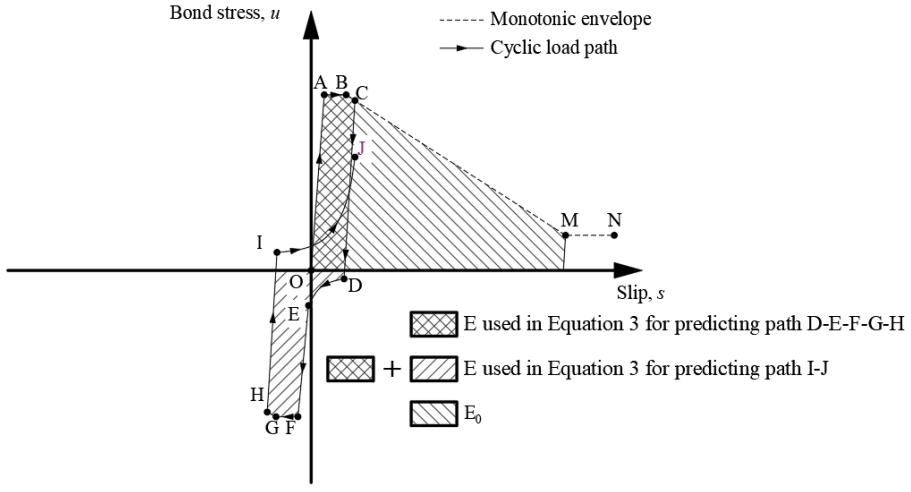

Fig. 17. Definition of dissipated energy under cyclic and monotonic loading.

UHPC-Vf1-PL-C-100D (Fig. 12e-g) because their responses were not affected by steel inelastic behavior. Following Equation 8 in Section 5.3, the steel deformation was subtracted from the LVDT readings (i.e., the measured displacement) to obtain the slip value that is used to calculate the energy term in Equation 3. Also shown in Fig. 18 is the damage index equation proposed by Eligehausen et al. [13] for concrete bond-slip behavior. The Eligehausen equation is developed based on cyclic bond tests of reinforced concrete with a compressive strength of around 30 MPa, while the UHPC tests used to determine Equation 3 had a compressive strength around 190 MPa. Compared to the Eligehausen equation, the faster damage growth featured by Equation 3 could be attributed to the higher brittleness of UHPC relative to traditional concrete [42].

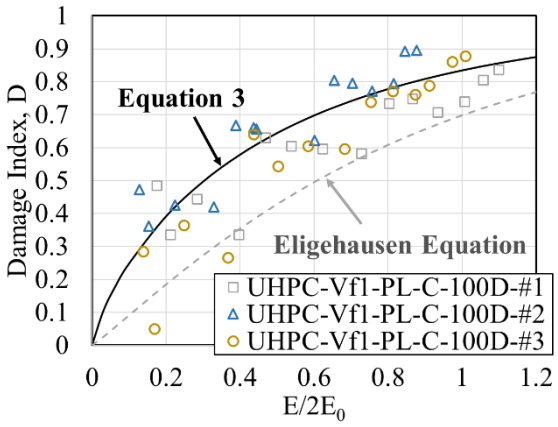

Fig. 18. Relationship between damage index and dissipated energy.

When a slip reversal starts, the bond-slip model first experiences a linear unloading branch with stiffness, E_b, until the frictional resistance, u_f, is reached (e.g., from C to D and from H to I in Fig. 16). Based on experimental results, the unloading stiffness, E_b, is typically 120 N/mm^3. The frictional resistance, u_f, is proposed as a function of damage index, D, and the experienced slip range:

$$u_f = 2.68 \cdot u_{bf} \cdot \ (S_{max} - S_{min})/S_3 \cdot (1 - D)^{1.4}, \ (S_{max} - S_{min}) \le S_3 \qquad (4)$$

, where S_{max}=maximum-experienced slip, and S_{min}=minimum-experienced slip, Fig. 16. Equation 4 is based on a regression analysis of the test results (Fig. 19) and experimental observations that the frictional resistance first increases with the increase of the experienced slip range, $S_{max} - S_{min}$, and then decreases as the internal damage becomes more severe. Also, under repeated cycles at similar slip values, the frictional resistance decreases as the internal damage increases.

After reaching the frictional resistance, the model follows a nonlinear reloading branch towards a reduced monotonic envelope (e.g., from point D to E and from I to J in Fig. 16). Following the suggestions of Filippou, et al. [43], the reloading branch is defined as a fourth-

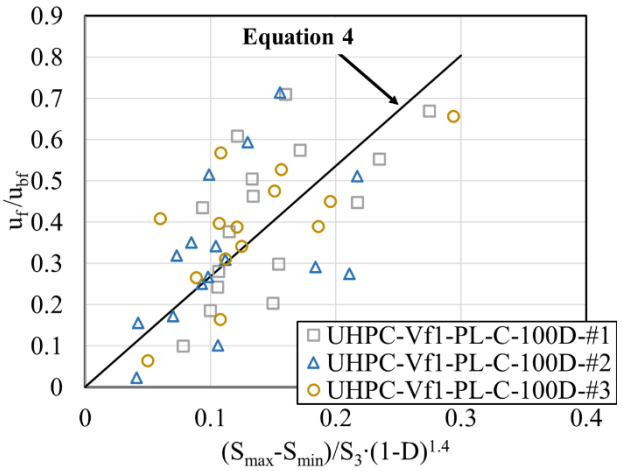

Fig. 19. Relationship between frictional resistance and damage index as well as experienced slip range.

degree polynomial function:

$$u(s) = \frac{u_E - u_S}{(s_E - s_S)^4} \cdot (s - s_S)^4 + u_S \quad (5)$$

, where s_S and u_S are the slip and bond stress values at the reloading starting point; s_E and u_E are the slip and bond stress values at the reloading end point.

During the first slip reversal, the reloading end point is defined as the point where the bond stress reaches four times the frictional resistance on the reduced envelope (e.g., point E in Fig. 16). During the following cycles, the reloading end point is defined as the point where the bond-slip reaches the maximum- or minimum-experienced slip (i.e., S_{max} or S_{min}) on the reduced envelope (e.g., point J in Fig. 16). After reaching the reloading ending point, the bond model will follow the reduced envelope until the next slip reversal begins (e.g., path E-F-G-H in Fig. 16).

Compared to the original monotonic envelope, the reduced envelope shares the same key slip value (i.e., s_1, s_2, s_3) but has smaller peak and residual strength:

$$u_{max,reduced} = (1 - D) \cdot u_{max} \quad (6)$$

$$u_{bf,reduced} = (1 - D) \cdot u_{bf} \quad (7)$$

5.3 Validation of the Proposed Bond-slip Model

Fig. 20 compares the monotonic bond-slip responses from the experiments and the model. Specimens that observed steel yielding are not included since their steel bar had inelastic deformation. The experimental slip is obtained by:

$$s = \Delta - L_s \cdot \varepsilon_s \quad (8)$$

, where Δ=averaged LVDT reading; L_s=distance between the LVDT clamping point and bond region; ε_s=steel strain, which is the ratio between steel stress and steel elastic modulus (Table 2).

In Fig. 20, the model adopts the averaged bond strength from the experimental results (Table 4). Fig. 20 demonstrates that, if the bond strength is correctly predicted, the proposed model well captures the initial ascending branch, gradual bond softening, and the residual frictional resistance.

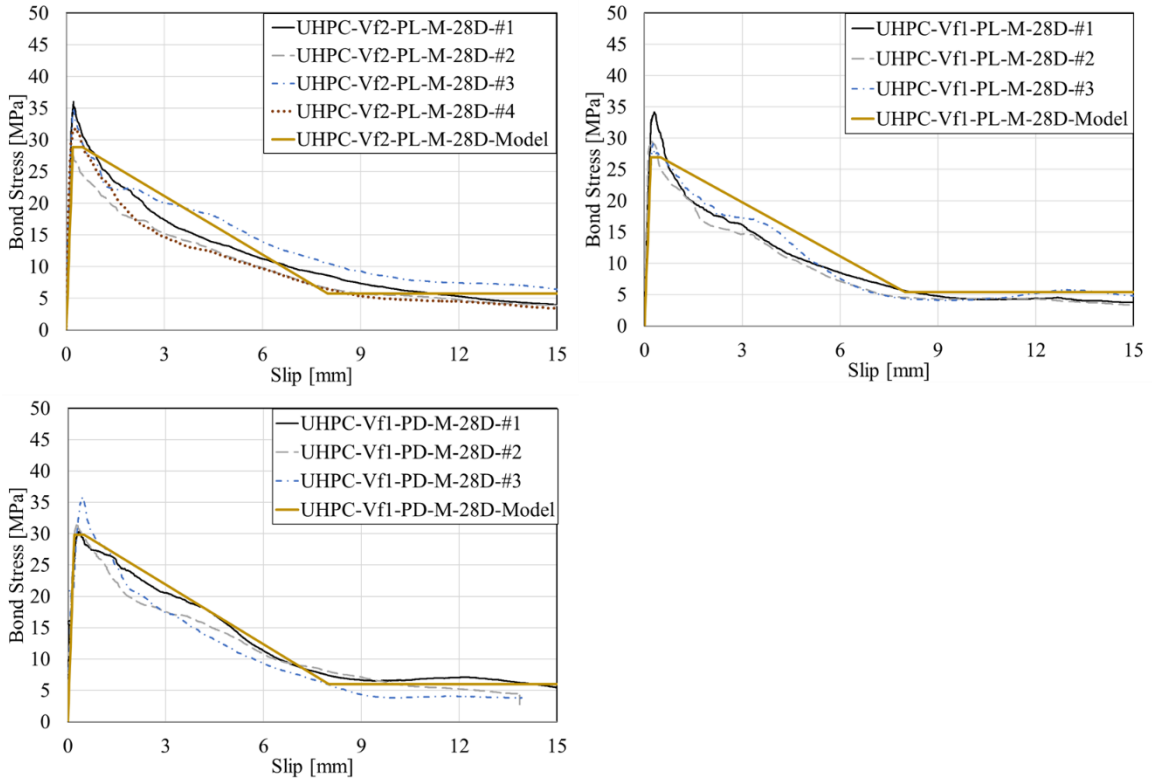

Fig. 20. Comparison between the prediction and monotonic experimental results.

Since the cyclic model parameters are obtained from regression analysis of results from UHPC-Vf1-PL-C-100D, the cyclic model is validated on test results from the same specimen type but with 2% volume fraction of fibers (i.e., UHPC-Vf2-PL-C-100D) as well as on beam-end test results from two additional types of HPFRCC: engineered cementitious composites (ECC) and self-consolidating high-performance fiber-reinforced concrete (SCHPFRC) [12]. For the two

UHPC specimens, the slip values are obtained by reducing the post-softening displacement (i.e., the black solid lines in Fig. 12a-b) by the elastic and inelastic steel deformation. The steel inelastic deformation is fixed upon bond softening (i.e., the transition from red dashed line to black solid lines in Fig. 12a-b), and steel elastic deformation is corrected using Equation 8. Fig. 21 compares the predicted cyclic responses to the experimental cyclic responses as well as the corresponding monotonic response. The mean absolute error of the predicted damage index, D, ranges from 11% to 13% for these four tests, indicating that the model reasonably captures the bond degradation under cyclic loading.

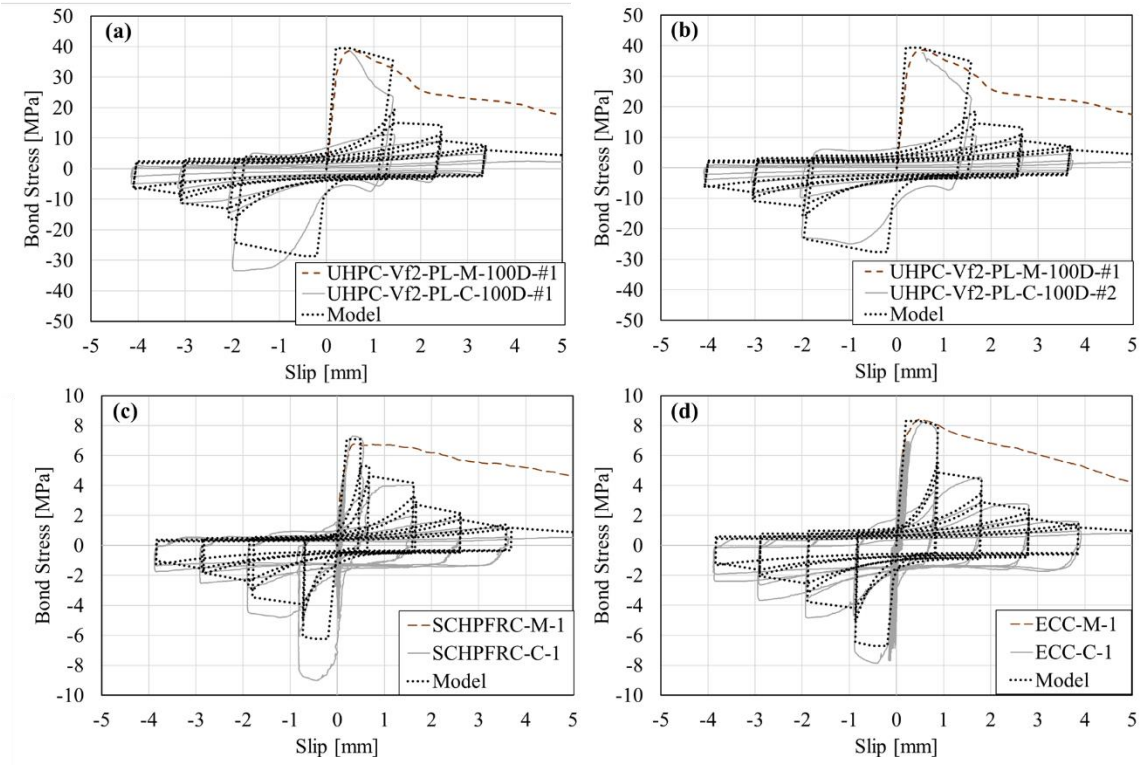

Fig. 21. Comparison between the predicted and experimental cyclic responses for (a) UHPC-Vf2-PL-M-100D-#1, (b) UHPC-Vf2-PL-M-100D-#2, (c) SCHPFR-C-1[12], (d) ECC-C-1 [12].

6 Conclusions

After reviewing the state-of-the-art of R/UHPC bond studies, this paper investigates the impact of fiber volume (1% or 2%), flow direction (parallel or perpendicular to the bar), and cyclic loading on R/UHPC bond behavior under flexural states. Current R/UHPC bond strength prediction methods are evaluated on test results from this study and the literature. A new bond-slip model for R/UHPC is proposed and validated. The following conclusions are reached:

1. For all four combinations of fiber volume and flow direction, R/UHPC exhibits confined splitting failure. Because splitting cracks are restrained by fiber-bridging, UHPC keys are sheared-off and pulverized.
2. Changing the flow direction from parallel flow to perpendicular flow (relative to the longitudinal axis of the bonded bar) increases the average bond strength by 9% and 26% for 1% fiber volume and 2% fiber volume, respectively.
3. Increasing the fiber volume from 1% to 2% increases the average bond strength by 9% and 26% for parallel flow and perpendicular flow, respectively.
4. Cyclic loading does not impact R/UHPC bond strength but accelerates bond degradation after bond softening occurs for the specimens studied here.
5. Current R/UHPC bond strength prediction methods, which are based on pullout tests and tension lap-splice tests, predict results from beam-type tests with a mean absolute error above 45%.
6. The proposed model captures the cyclic bond degradation of R/UHPC and other types of HPFRCC under flexural stress states with a mean absolute error under 13%.

More beam-type tests are needed to evaluate R/UHPC bond behavior with a wider range of material properties and geometries (e.g., cover thickness and reinforcing bar diameters). A validated method for predicting R/UHPC bond strength under flexural states is needed.

7 Acknowledgements

The authors are grateful for the financial support from the John A. Blume Earthquake Engineering Center and the Stanford Vice Provost for Undergraduate Education (Summer interns). The authors gratefully acknowledge Headed Reinforcement Corp., CA for fabricating the coupler-headed steel bars. The authors appreciate the cylinder end-grinding service at the concrete material lab of California Department of Transportation, Sacramento.
The authors deeply appreciate the technical support provided by Dr. Kyle Douglas and Mr. Bill Sabala.

8 CRediT Author Statement

Yi Shao: Conceptualization, Methodology, Investigation, Analysis, Writing-Original Draft. **Katie Tich:** Investigation. **Sandro Boaro:** Investigation. **Sarah Billington:** Supervision, Writing-Review & Editing, Funding acquisition.

9 Declaration of Interest

None.

Appendix A

	f_c (MPa)	Fiber	V_f	f_t (MPa)	d_b (mm)	c/d_b	l_b/d_b	Test type	Failure Type	u_{max} (MPa)
[20]	171	SF	2.0%	NA	16.0	1.3	2.0	Pull-out	Pull out + Splitting	39.5
	155	SF	2.0%	NA	16.0	1.3	2.0	Pull-out	Pull out	49.9
	171	SF	2.0%	NA	16.0	3.1	2.0	Pull-out	Pull out	56.0
	155	SF	2.0%	NA	16.0	3.1	2.0	Pull-out	Pull out	57.3
	171	SF	2.0%	NA	16.0	4.7	2.0	Pull-out	Pull out	60.6
	155	SF	2.0%	NA	16.0	4.7	2.0	Pull-out	Pull out	57.0
[23]	70.7	SF	2.0%	6.0	16.0	1.6	8.0	TLS	Splitting	7.4
	70.7	SF	2.0%	6.0	16.0	1.6	10.0	TLS	Splitting	8.0
	70.7	SF	2.0%	6.0	16.0	1.6	12.0	TLS	Splitting	9.0
	70.7	SF	2.0%	6.0	16.0	1.6	14.0	TLS	Splitting	7.7
	70.7	SF	2.0%	6.0	16.0	3.1	8.0	TLS	Splitting	11.4
	70.7	SF	2.0%	6.0	16.0	3.1	10.0	TLS	Splitting	12.2
	70.7	SF	2.0%	6.0	16.0	3.1	12.0	TLS	Splitting	13.4
	74.9	SF	2.0%	7.0	16.0	1.6	8.0	TLS	Splitting	7.1
	74.9	SF	2.0%	7.0	16.0	1.6	10.0	TLS	Splitting	8.0
	74.9	SF	2.0%	7.0	16.0	1.6	12.0	TLS	Splitting	8.5
	74.9	SF	2.0%	7.0	16.0	1.6	14.0	TLS	Splitting	8.2
	74.9	SF	2.0%	7.0	16.0	3.1	8.0	TLS	Splitting	9.7
	74.9	SF	2.0%	7.0	16.0	3.1	10.0	TLS	Splitting	11.3

	74.9	SF	2.0%	7.0	16.0	3.1	12.0	TLS	Splitting	12.4
[26]	161	SF	1.0%	9.2	9.5	2.2	8.0	TLS	Splitting	17.9
	161	SF	2.0%	13.4	9.5	2.2	8.0	TLS	Splitting	24.0
	161	SF	3.0%	19.1	9.5	2.2	8.0	TLS	Splitting	32.2
	161	SF	1.0%	9.2	9.5	2.2	12.0	TLS	Splitting	15.0
	161	SF	2.0%	13.4	9.5	2.2	12.0	TLS	Splitting	16.9
	161	SF	2.0%	13.4	9.5	2.2	12.0	TLS	Splitting	20.5
	161	SF	2.0%	13.4	9.5	2.2	12.0	TLS	Splitting	23.0
	161	SF	1.0%	9.2	9.5	2.2	16.0	TLS	Splitting	15.2
	161	SF	1.0%	9.2	12.7	1.5	8.0	TLS	Splitting	14.3
	161	SF	2.0%	13.4	12.7	1.5	8.0	TLS	Splitting	22.1
	161	SF	3.0%	19.1	12.7	1.5	8.0	TLS	Splitting	24.2
	161	SF	1.0%	9.2	12.7	1.5	12.0	TLS	Splitting	11.4
	161	SF	2.0%	13.4	12.7	1.5	12.0	TLS	Splitting	11.2
	161	SF	2.0%	13.4	12.7	1.5	12.0	TLS	Splitting	15.3
	161	SF	2.0%	13.4	12.7	1.5	12.0	TLS	Splitting	16.2
	161	SF	3.0%	19.1	12.7	1.5	12.0	TLS	Splitting	19.4
[25]	191	SF	2.0%	NA	13.0	5.3	4.0	Pull-out	Splitting	32.7
	191	SF	2.0%	NA	13.0	5.3	4.0	Pull-out	Splitting	26.2
	189.4	SF	2.0%	NA	16.0	4.2	6.4	Pull-out	Splitting	16.6
	189.4	SF	2.0%	NA	16.0	4.2	6.4	Pull-out	Splitting	17.9
	188.9	SF	2.0%	NA	16.0	4.2	4.8	Pull-out	Splitting	17.8
	188.9	SF	2.0%	NA	16.0	4.2	4.8	Pull-out	Splitting	19.1
	191	SF	2.0%	NA	16.0	4.2	3.2	Pull-out	Splitting	31.0
	191	SF	2.0%	NA	16.0	4.2	3.2	Pull-out	Splitting	31.2
	189.4	SF	2.0%	NA	19.0	3.4	5.3	Pull-out	Splitting	14.4
	189.4	SF	2.0%	NA	19.0	3.4	5.3	Pull-out	Splitting	15.0
	188.9	SF	2.0%	NA	19.0	3.4	4.0	Pull-out	Splitting	17.6
	188.9	SF	2.0%	NA	19.0	3.4	4.0	Pull-out	Splitting	19.1
	191	SF	2.0%	NA	19.0	3.4	2.6	Pull-out	Splitting	23.0
	191	SF	2.0%	NA	19.0	3.4	2.6	Pull-out	Splitting	23.2
	188.9	SF	2.0%	NA	19.0	3.4	4.0	Pull-out	Splitting	15.1
	188.9	SF	2.0%	NA	16.0	4.2	6.4	Pull-out	Splitting	18.3

	52.8	SF	2.0%	NA	16.0	4.2	6.4	Pull-out	Splitting	10.1
	88	SF	2.0%	NA	16.0	4.2	6.4	Pull-out	Splitting	11.1
	124.6	SF	2.0%	NA	16.0	4.2	6.4	Pull-out	Splitting	14.6
	180.1	SF	1.0%	NA	16.0	4.2	6.4	Pull-out	Splitting	14.8
	188.9	SF	2.0%	NA	16.0	4.2	6.4	Pull-out	Splitting	17.6
	180.1	SF	1.0%	NA	19.0	3.4	4.0	Pull-out	Splitting	11.1
[27]	94.5	SF	2.0%	NA	16.0	2.0	8.0	TLS	Splitting	17.8
	94.5	SF	2.0%	NA	16.0	3.5	8.0	TLS	Splitting	22.8
	132	SF	2.0%	NA	16.0	2.0	6.0	TLS	Splitting	22.9
	94.5	SF	2.0%	NA	16.0	2.0	8.0	TLS	Splitting	22.6
	94.5	SF	2.0%	NA	16.0	3.5	8.0	TLS	Splitting	30.2
	132	SF	2.0%	NA	16.0	2.0	6.0	TLS	Splitting	26.3
[21]	205	SF+PP	2.5%	13.9	8.0	2.5	4.0	Pull-out	Pull out	38.3
	205	SF+PP	2.5%	13.9	12.0	1.7	4.0	Pull-out	Splitting + Pull out	32.9
	205	SF+PP	2.5%	13.9	12.0	1.7	4.0	Pull-out	Pull out	36.5
	205	SF+PP	2.5%	13.9	12.0	1.7	8.0	Pull-out	Splitting + Pull out	37.1
	205	SF+PP	2.5%	13.9	12.0	2.5	4.0	Pull-out	Pull out	36.5
	205	SF+PP	2.5%	13.9	12.0	2.5	4.0	Pull-out	Pull out	36.8
	205	SF+PP	2.5%	13.9	12.0	2.5	4.0	Pull-out	Pull out	36.6
	205	SF+PP	2.5%	13.9	12.0	16.2	2.5	Pull-out	Pull out	54.9
	205	SF+PP	2.5%	13.9	12.0	16.2	2.5	Pull-out	Pull out	52.1
	205	SF+PP	2.5%	13.9	12.0	16.2	2.5	Pull-out	Pull out	53.3
	205	SF+PP	2.5%	13.9	16.0	12.0	2.5	Pull-out	Pull out	59.1
	205	SF+PP	2.5%	13.9	16.0	12.0	2.5	Pull-out	Pull out	59.3
	205	SF+PP	2.5%	13.9	16.0	12.0	2.5	Pull-out	Pull out	50.2
[44]	132.3	SF	1.0%	10.0	25.0	1.2	5.0	TLS	Splitting	6.6
	138	SF	1.0%	5.7	25.0	1.2	10.0	TLS	Splitting	7.0
	119.6	SF	2.0%	5.3	25.0	1.2	5.0	TLS	Splitting	8.1
	126.3	SF	2.0%	8.3	25.0	1.2	10.0	TLS	Splitting	8.5

	115.5	SF	4.0%	8.1	25.0	1.2	5.0	TLS	Splitting	11.0
	106.2	SF	4.0%	12.8	25.0	1.2	8.0	TLS	Splitting	10.8
	115.1	SF	4.0%	10.5	25.0	1.2	10.0	TLS	Splitting	10.3
[38]	104	SF	4.0%	13.0	25.0	1.2	5.0	TLS	Splitting	10.3
	115	SF	4.0%	9.3	25.0	1.2	5.0	TLS	Splitting	11.0
	106	SF	4.0%	12.8	25.0	1.2	8.0	TLS	Splitting	10.8
	115	SF	4.0%	10.5	25.0	1.2	10.0	TLS	Splitting	10.3
	135	SF	4.0%	13.0	35.0	1.2	5.0	TLS	Splitting	11.7
	135	SF	4.0%	13.9	35.0	1.2	10.0	TLS	Splitting	11.0
	120	SF	2.0%	13.9	25.0	1.2	5.0	TLS	Splitting	8.1
	126	SF	2.0%	8.3	25.0	1.2	10.0	TLS	Splitting	8.5
	153	SF	2.0%	8.1	35.0	1.2	5.0	TLS	Splitting	8.1
	153	SF	2.0%	9.0	35.0	1.2	10.0	TLS	Splitting	9.6
	132	SF	1.0%	9.0	25.0	1.2	5.0	TLS	Splitting	6.6
	138	SF	1.0%	5.7	25.0	1.2	10.0	TLS	Splitting	7.0
	167	SF	1.0%	5.3	35.0	1.2	5.0	TLS	Splitting	6.9
	167	SF	1.0%	6.3	35.0	1.2	10.0	TLS	Splitting	7.2
[45]	196.4	SF	2.0%	6.3	16.0	4.2	1.0	Pull-out	Pull out	64.0
	196.4	SF	2.0%	7.4	16.0	4.2	1.5	Pull-out	Pull out	72.0
	196.4	SF	2.0%	7.4	16.0	4.2	2.0	Pull-out	Pull out	68.8
[35]	196.8	SF	1.0%	7.4	16.0	4.2	1.0	Pull-out	Pull out	66.7
	196.8	SF	1.0%	8.2	16.0	4.2	2.0	Pull-out	Pull out	68.2
	201.8	SF	2.0%	8.2	16.0	4.2	1.0	Pull-out	Pull out	74.6
	201.8	SF	2.0%	11.8	16.0	4.2	2.0	Pull-out	Pull out	70.9
	207.2	SF	3.0%	11.8	16.0	4.2	1.0	Pull-out	Pull out	76.3
	207.2	SF	3.0%	14.2	16.0	4.2	2.0	Pull-out	Pull out	71.8
	184.9	SF	4.0%	14.2	16.0	4.2	1.0	Pull-out	Pull out	68.3
	184.9	SF	4.0%	16.6	16.0	4.2	2.0	Pull-out	Pull out	71.1
[41]	120.7	SF	6.0%	16.6	20.0	1.5	10.0	BLS	Splitting	11.6
[46]	NA	SF	2.5%	10.5	20.0	3.5	2.5	Pull-out	Pull out	54.0
	NA	SF	2.5%	9.7	20.0	3.5	2.0	Pull-out	Pull out	66.0
	NA	SF	2.5%	9.7	12.0	6.2	1.7	Pull-out	Pull out	61.0
[47]	155	SF	1.0%	9.7	14.0	1.5	NA	Pull-out	Splitting	19.9

	155	SF	1.0%	NA	14.0	2.0	NA	Pull-out	Splitting	26.8
	155	SF	1.0%	NA	18.0	1.5	NA	Pull-out	Splitting	17.3
	155	SF	1.0%	NA	18.0	2.0	NA	Pull-out	Splitting	25.3

Note: f_c=UHPC compressive strength; V_f=fiber volume; d_b=bar diameter; c=cover thickness, l_b=bonded length; u_{max}=peak bond strength; SF=Steel fiber; PP=Polypropylene fiber; TLS =Tension lap-splice; BLS=Beam lap-splice; NA=Not available.

10 References

[1] Haber ZB, De la Varga I, Graybeal BA, Nakashoji B, El-Helou R. Properties and Behavior of UHPC-Class Materials. FHWA-HRT-18-036. 2018.

[2] Naaman AE, Reinhardt H-W. Proposed classification of HPFRC composites based on their tensile response. Mater Struct. 2006;39:547-55.

[3] Shao Y, Shao X, Li L, Wu J. Optimum Combination of Bridge and Deck Systems for Superspan Cable-Stayed Bridges. Journal of Bridge Engineering. 2018;23:04017112.

[4] Russell HG, Graybeal BA. Ultra-high performance concrete: A state-of-the-art report for the bridge community. FHWA; 2013.

[5] Thomas M, Green B, O'Neal E, Perry V, Hayman S, Hossack A. Marine performance of UHPC at Treat Island. Proceedings of the 3rd International Symposium on UHPC and Nanotechnology for High Performance Construction Materials, Kassel, Germany2012. p. 365-70.

[6] Fehling E, Schmidt M, Walraven J, Leutbecher T, Fröhlich S. Ultra-high performance concrete UHPC: Fundamentals, design, examples: John Wiley & Sons; 2014.

[7] Zhou B, Uchida Y. Influence of flowability, casting time and formwork geometry on fiber orientation and mechanical properties of UHPFRC. Cement and Concrete Research. 2017;95:164-77.

[8] Walsh K, Hicks N, Steinberg E, Hussein H, Semendary A. Fiber Orientation in Ultra-High-Performance Concrete Shear Keys of Adjacent-Box-Beam Bridges. ACI Mater J. 2018;115.

[9] Bastien-Masse M, Denarié E, Brühwiler E. Effect of fiber orientation on the in-plane tensile response of UHPFRC reinforcement layers. Cement and Concrete Composites. 2016;67:111-25.

[10] Duque LFM, Graybeal B. Fiber orientation distribution and tensile mechanical response in UHPFRC. Mater Struct. 2017;50:55.

[11] Huang L, Chi Y, Xu L, Chen P, Zhang A. Local bond performance of rebar embedded in steel-polypropylene hybrid fiber reinforced concrete under monotonic and cyclic loading. Constr Build Mater. 2016;103:77-92.

[12] Bandelt MJ, Frank TE, Lepech MD, Billington SL. Bond behavior and interface modeling of reinforced high-performance fiber-reinforced cementitious composites. Cement and Concrete Composites. 2017;83:188-201.

[13] Eligehausen R, Popov EP, Bertero VV. Local bond stress-slip relationships of deformed bars under generalized excitations: experimental results and analytical model. 1983.

[14] Hung C-C, Chueh C-Y. Cyclic behavior of UHPFRC flexural members reinforced with high-strength steel rebar. Eng Struct. 2016;122:108-20.

[15] Xu S, Wu C, Liu Z, Han K, Su Y, Zhao J et al. Experimental investigation of seismic behavior of ultra-high performance steel fiber reinforced concrete columns. Eng Struct. 2017;152:129-48.

[16] Hung C-C, Hsieh P-L. Comparative study on shear failure behavior of squat high-strength steel reinforced concrete shear walls with various high-strength concrete materials. Structures. 2020;23:56-68.

[17] Shao Y. Improving Ductility and Design Methods of Reinforced High-Performance Fiber-Reinforced Cementitious Composite (HPFRCC) Flexural Members. Stanford: Stanford University; 2020.

[18] 408 AC. Bond and Development of Straight Reinforcing Bars in Tension. 2003.
[19] Yoo D-Y, Shin H-O. Bond performance of steel rebar embedded in 80–180 MPa ultra-high-strength concrete. Cement and Concrete Composites. 2018;93:206-17.
[20] Sturm AB, Visintin P. Local bond slip behavior of steel reinforcing bars embedded in ultra high performance fibre reinforced concrete. Structural Concrete. 2019;20:108-22.
[21] Marchand P, Baby F, Khadour A, Battesti T, Rivillon P, Quiertant M et al. Bond behaviour of reinforcing bars in UHPFRC. Mater Struct. 2016;49:1979-95.
[22] Ronanki VS, Aaleti S, Valentim DB. Experimental investigation of bond behavior of mild steel reinforcement in UHPC. Eng Struct. 2018;176:707-18.
[23] Zhou Z, Qiao P. Bond behavior of epoxy-coated rebar in ultra-high performance concrete. Constr Build Mater. 2018;182:406-17.
[24] Kim JS, Park JH. An Experiment on Bond Properties of Reinforcements Embedded in Ultra High Performance Concrete. Materials Science Forum: Trans Tech Publ; 2016. p. 323-6.
[25] Alkaysi M, El-Tawil S. Factors affecting bond development between Ultra High Performance Concrete (UHPC) and steel bar reinforcement. Constr Build Mater. 2017;144:412-22.
[26] Roy M, Hollmann C, Wille K. Influence of volume fraction and orientation of fibers on the pullout behavior of reinforcement bar embedded in ultra high performance concrete. Constr Build Mater. 2017;146:582-93.
[27] Yuan J, Graybeal B. Bond of Reinforcement in Ultra-High-Performance Concrete. ACI Struct J. 2016;113:1130.
[28] Čítek D, Huňka P, Řeháček S, Mandlík T, Kolísko J. Testing of bond behavior of UHPC. Advanced Materials Research: Trans Tech Publ; 2014. p. 95-8.
[29] Moreno DM, Trono W, Jen G, Ostertag C, Billington SL. Tension stiffening in reinforced high performance fiber reinforced cement-based composites. Cement and Concrete Composites. 2014;50:36-46.
[30] Hung C-C, Lee H-S, Chan SN. Tension-stiffening effect in steel-reinforced UHPC composites: Constitutive model and effects of steel fibers, loading patterns, and rebar sizes. Composites Part B: Engineering. 2019;158:269-78.
[31] Shao Y, Billington SL. Predicting the two predominant flexural failure paths of longitudinally reinforced high-performance fiber-reinforced cementitious composite structural members. Eng Struct. 2019;199:109581.
[32] Shao Y, Billington SL. Impact of cyclic loading on longitudinally-reinforced UHPC flexural members with different fiber volumes and reinforcing ratios. Eng Struct. 2021;241:112454.
[33] C1856 A. Standard Practice for Fabricatingand Testing Specimens of Ultra-High Performance Concrete. 2017.
[34] ASTM. ASTM A944-10 Comparing Bond Strength of Steel Reinforcing Bars to Concrete Using Beam-End Specimens. 2010.
[35] Yoo D-Y, Shin H-O, Yang J-M, Yoon Y-S. Material and bond properties of ultra high performance fiber reinforced concrete with micro steel fibers. Composites Part B: Engineering. 2014;58:122-33.
[36] Shao Y, Billington SL. Bond Performance of Ultra-High-Performance Concrete (UHPC) Under Flexural States. Proceedings of fib Symposium 2021. Lisbon, Portugal2021.

[37] Deng M, Pan J, Sun H. Bond behavior of deformed bar embedded in Engineered Cementitious Composites under cyclic loading. Constr Build Mater. 2019;197:164-74.
[38] Lagier F, Massicotte B, Charron JP. Bond strength of tension lap splice specimens in UHPFRC. Constr Build Mater. 2015;93:84-94.
[39] Concrete IFfS. Fib Model Code for Concrete Structures 2010. Berlin, Germany: Ernst & Sohn; 2010.
[40] Groeneveld AB, Ahlborn TM, Crane CK, Burchfield CA, Landis EN. Dynamic strength and ductility of ultra-high performance concrete with flow-induced fiber alignment. Int J Impact Eng. 2018;111:37-45.
[41] Maya LF, Zanuy C, Albajar L, Lopez C, Portabella J. Experimental assessment of connections for precast concrete frames using ultra high performance fibre reinforced concrete. Constr Build Mater. 2013;48:173-86.
[42] Ju Y, Liu HB, Chen J, Jia YD, Peng PH. Toughness and characterization of reactive powder concrete with ultra-high strength. Sci China Ser E-Technol Sci. 2009;52:1000-18.
[43] Filippou FC, Bertero VV, Popov EP. Effects of bond deterioration on hysteretic behavior of reinforced concrete joints. 1983.
[44] Lagier F, Massicotte B, Charron J-P. Experimental investigation of bond stress distribution and bond strength in unconfined UHPFRC lap splices under direct tension. Cement and Concrete Composites. 2016;74:26-38.
[45] Yoo D-Y, Park J-J, Kim S-W, Yoon Y-S. Influence of reinforcing bar type on autogenous shrinkage stress and bond behavior of ultra high performance fiber reinforced concrete. Cement and Concrete Composites. 2014;48:150-61.
[46] Jungwirth J, Muttoni A. Structural behavior of tension members in Ultra High Performance Concrete. International symposium on ultra high performance concrete: International Symposium on Ultra High Performance Concrete; 2004.
[47] Cattaneo S, Rosati G. Bond and splitting in high performance fiber reinforced concrete. Proceedings of the Fifth International RILEM Symposium on Fiber-Reinforced Concretes (FRC), BEFIB'20002000.